Updated data of the 153 Galactic globular clusters are used to readdress fundamental parameters of the Milky Way, such as the distance of the Sun to the Galactic center, bulge and halo structural parameters and cluster destruction rates. We build a reduced sample, decontaminated of the clusters younger than 10 Gyr, those with retrograde orbits and/or evidence of relation to dwarf galaxies. The reduced sample contains 116 globular clusters that are tested whether formed in the primordial collapse. The 33 metal-rich globular clusters ([Fe/H] ≥ -0.75) of the reduced sample extend basically to the Solar circle and distribute over a region with projected axial-ratios typical of an oblate spheroidal, $\Delta x : \Delta y : \Delta z \approx 1.0 : 0.9 : 0.4$. Those outside this region appear to be related to accretion. The 81 metal-poor globular clusters span a nearly spherical region of axial-ratios $\approx 1.0 : 1.0 : 0.8$ extending from the central parts to the outer halo, although several clusters in the external region still require detailed studies to unravel their origin as accretion or collapse. A new estimate of the Sun's distance to the Galactic center based on symmetries of the spatial distribution of 116 globular clusters is provided with an uncertainty considerably smaller than in previous determinations using globular clusters, $R_O = 7.2 \pm 0.3$ kpc. The metal-rich and metal-poor radial-density distributions flatten for $R_{GC} \leq 2$ kpc and are well represented over the full Galactocentric distance range both by a power-law with a core-like term and Sérsic's law; at large distances they fall off as $\sim R^{-3.9}$. Both metallicity components appear to have a common origin, which is different from that of the dark matter halo. Structural similarities of the metal-rich and metal-poor radial distributions with the stellar halo are consistent with a scenario where part of the reduced sample was formed in the primordial collapse, and part was accreted in an early period of merging. This applies to the bulge as well, suggesting an early merger affecting the central parts of the Galaxy. The present decontamination procedure is not sensitive to all accretions (especially prograde) during the first Gyrs, since the observed radial density profiles still preserve traces of the earliest merger(s). We estimate that the present globular cluster population corresponds to $\leq 23 \pm 6\%$ of the original one. The fact that the volume-density radial distributions of the metal-rich and metal-poor globular clusters of the reduced sample follow both a core-like power-law and Sérsic's law indicates that we are dealing with spheroidal subsystems in all scales.

Key words. (*Galaxy:*) globular clusters: general; *Galaxy:* structure

Astronomy & Astrophysics manuscript no. GCS February 5, 2008
(DOI: will be inserted by hand later)

Globular cluster system and Milky Way properties revisited

E. Bica[1], C. Bonatto[1], B. Barbuy[2], and S. Ortolani[3]

[1] Universidade Federal do Rio Grande do Sul, Instituto de Física, CP 15051, Porto Alegre 91501-970, RS, Brazil
e-mail: bica@if.ufrgs.br, charles@if.ufrgs.br
[2] Universidade de São Paulo, Dept. de Astronomia, Rua do Matão 1226, São Paulo 05508-090, Brazil
e-mail: barbuy@astro.iag.usp.br
[3] Università di Padova, Dipartimento di Astronomia, Vicolo dell'Osservatorio 2, I-35122 Padova, Italy
e-mail: ortolani@pd.astro.it

Received –; accepted –

Abstract.

1. Introduction

Globular clusters (GCs) are potential witnesses of the formation processes that gave rise to the Milky Way. Because of their long-lived nature, GCs formed in the initial phases of the Galaxy may preserve in their structure and spatial distribution information that is essential to probe these early conditions. In this sense, derivation of the present-day spatial distribution of GCs as well as their physical properties can be used to infer on the Galaxy formation and evolution processes and better trace out the geometry of the Galaxy.

Early models suggested that the Galaxy formed as a consequence of a monolithic, dissipative collapse of a single massive, nearly-spherical spinning gas cloud (e.g. Eggen, Lynden-Bell & Sandage 1962; Sandage 1990). Initial conditions of the collapse included low-metallicity gas and a nearly free-fall regime. This process should be reflected in the GC population as a homogeneity in certain parameters, such as orbital motions and a restricted age range. However, later work presented observational evidence that the present-day GC population results not only from the primordial collapse but from merging and captures of smaller neighbouring galaxies early in the history of the Galaxy (Searle & Zinn 1978; Zinn 1980) or in more recent events such as the accretion and disruption of the Sagittarius dwarf spheroidal galaxy (Ibata, Irwin & Gilmore 1994; Ibata et al. 1997). On theoretical grounds, N-body simulations (using standard cosmological conditions such as cold dark matter) suggest that the hierarchical merging of satellites might be the main building blocks of galaxy formation (Bellazzini, Ferraro & Ibata 2003).

Present-day data picture the region interior to $\sim$ 10 kpc (inner halo/bulge) as formed essentially by the primordial dissipative collapse (e.g. van den Bergh & Mackey 2005), while the region external to $\sim$ 15 kpc (outer halo) was formed by later infall and capture of smaller fragments (Searle & Zinn 1978; Zinn 1993). Mackey & Gilmore (2004) and Mackey & van den Bergh (2005) studied the properties of GCs by means of the horizontal-branch morphology, photometric and structural parameters. They found significant differences among age/metallicity subgroups. Mackey & Gilmore (2004) reported that $\sim$ 30% of the Milky Way GCs have properties similar to those of the GCs in the LMC, SMC, Fornax and Sagittarius dwarf spheroidal galaxies. This suggests that a significant fraction of the Galactic GC population, in particular outer halo ones, has an extragalactic origin.

Regardless of the origin, the Galaxy contains $\sim$ 150 GCs that are characterized by a bimodal metallicity distribution, and distances to the Galactic center of up to $\sim$ 150 kpc. With respect to the metallicity vs. position relation, the metal-rich GCs used to be associated with a disk while the metal-poor ones with the halo (Kinman 1959; Zinn 1985; Armandroff 1989). More recently the metal-rich GCs have been found to characterize a bulge population (Minniti 1995; Barbuy et al. 1999; Coté 1999; van den Bergh 2000). Chemical enrichment models of the Galaxy, especially for the central parts (Matteucci & Romano 1999; Matteucci, Romano & Molaro 1999), predict that the formation of the bulge occurred from the same gas, but even faster than the inner halo.

Considerable efforts have been undertaken in the last $\sim$ 15 years to obtain fundamental parameters of globular clusters by means of accurate CCD colour-magnitude diagrams e.g. for the central parts of the Galaxy (Barbuy,

Send offprint requests to: C. Bonatto

Bica & Ortolani 1998). Harris (1996), as updated[1] in 2003 (and references therein), compiled parameters of GCs that we will adopt as the starting point for this work. Hereafter we refer to Harris' database as H03.

Previous work have focused on the study of global properties and correlations among intrinsic parameters of the Galactic GC system, including as well the search for correlations with position in the Galaxy, e.g. Djorgovski & Meylan (1994), van den Bergh (2003) and Mackey & van den Bergh (2005).

The significant improvement in the observational GC data is in itself a reason for checking if classically adopted values related to the early formation of the Galaxy and the GC system are still valid. In the present study we use an updated set of GC parameters, e.g. reddening, metallicity, distance from the Sun, age and orbital motion to address their spatial distribution. Since one of the latest derivations of the Galactic center distance using GCs was made by Reid (1993) we also discuss that value now based on the updated GC data.

Our basic approach is to decontaminate the GC sample of the clusters clearly not related to the primordial collapse of the Galaxy. We do this by identifying young GCs, those with retrograde orbits and/or related to the accretion of dwarf satellite galaxies.

This paper is organized as follows. In Sect. 2 we present the updated GC sample and isolate the clusters probably associated to the primordial collapse. In Sect. 3 we present projections of their positions onto the (x,y), (x,z) and (y,z) planes, derive the distance to the Galactic center and infer on Galactic structure. In Sect. 4 we build GC radial density profiles, fit them with different analytical functions and discuss GC destruction rates. In Sect. 5 we discuss a possible scenario to account for the present spatial distribution of GCs. Concluding remarks are given in Sect. 6.

2. The updated globular cluster data set

In the last 10 years new entries have been added to the census of Galactic GCs either by means of discoveries or identifications of misclassified open clusters, e.g. IC 1257 (Harris et al. 1997), ESO 280-SC06 (Ortolani, Bica & Barbuy 2000), 2MASS-GC01 and GC02 (Hurt et al. 2000), GLIMPSE-C01 (Kobulnicky et al. 2005), the diffuse cluster-type object SDSSJ1049 + 5103 (Willman et al. 2005), and the recently re-classified GC Whiting 1 (Carraro 2005). For new and already known GCs H03 has provided constant updating of fundamental parameters.

Parameters of the 153 presently known GCs in the Galaxy are listed in Table 1. We complemented the H03 database by adding information on new GCs in the last 2 years as indicated in the notes to Table 1. The presently updated GC data set will be hereafter referred to as the GC05 sample.

To estimate errors in distance determinations for the subsequent analyses we took into account GC05 and typical distance errors in the literature which are dominated by reddening uncertainties (e.g. Barbuy, Bica & Ortolani 1998). We adopt the following values for the reddening and distance error relation: $\varepsilon = 0.05$ for $E(B-V) \leq 0.2$, $\varepsilon = 0.10$ for $0.2 < E(B-V) \leq 0.8$, $\varepsilon = 0.15$ for $0.8 < E(B-V) \leq 1.5$, $\varepsilon = 0.2$ for $1.5 < E(B-V) \leq 2.0$, and $\varepsilon = 0.25$ for $E(B-V) \geq 2.0$, where ε is the fractional error in distance. Uncertainties in related parameters are obtained by propagation of ε.

As discussed in Sect. 1, the Galactic GC system is not expected to be homogeneous in terms of cluster origin. Since we intend to base our analysis on GCs with a high probability of formation in the primordial collapse, we exclude from GC05 those with evidence either of extragalactic origin or formation later than the collapse. To this category belong the GCs with retrograde orbits (e.g. Dinescu, Girard & van Altena 1999), ages younger than 10 Gyr (e.g. Salaris & Weiss 2002), direct relation or tidal debris of dwarf galaxies (e.g. Forbes, Strader & Brodie 2004) and finally, luminous GCs with evidence of being accreted dwarf galaxy nuclei (e.g. Mackey & van den Bergh 2005). References are given in col. 12 of Table 1. We found that 37 GCs (24% of GC05) fit into one or more of these categories. The remaining 116 GCs are part of what we define hereafter as the reduced sample (RS-GC05). One caveat with respect to the decontamination process is that it certainly is not sensitive to all events, accretions in particular, dating back to the first Gyrs of the Galaxy. For instance, extragalactic GCs accreted in this period with prograde orbits would in the present hardly be distinguishable from the Milky Way's native population.

Table 1 contains, by columns: (1) - main GC designation; (2) and (3) - Galactic coordinates; (4) - reddening; (5) - metallicity; (6) - distance from the Sun; (7) - input Galactocentric distance; (8) - output Galactocentric distance (Sect. 3.1); (9)–(11) - input Heliocentric components (Sect. 3); (12) - indicators of non-collapse membership; and (13) - additional GC designations as compiled from the literature by one of us (E.B.).

In Fig. 1 (upper panels) we compare the globular clusters of RS-GC05 with those in GC05 in terms of metallicity. The well-known bimodal distribution in metallicity (seen e.g. as early as in Zinn 1985) is confirmed not only in the present GC05 sample (panel (a)) but also in RS-GC05 (panel (b)), however with a smaller amplitude ratio between the metal-rich and metal-poor GCs. In the subsequent analysis we adopt $[Fe/H] = -0.75$ as the metallicity threshold between metal-rich and metal-poor[2] GCs. RS-GC05 contains 81 metal-poor GCs, 33 metal-rich and 2 with unknown metallicity (2MASS-GC02 and GLIMPSE-C01). The reddening distribution of the RS-GC05 GCs (panel (c)) is compared to those of the corresponding metal-poor (panel (d)) and metal-rich GCs (panel (e)). The reddening distribution of the metal-poor GCs presents a maximum around $E(B-V) \approx 0.05$ and

[1] at http://physun.physics.mcmaster.ca/Globular.html

[2] For simplicity we refer as metal-poor GCs the genuine together with the intermediate-metallicity ones.

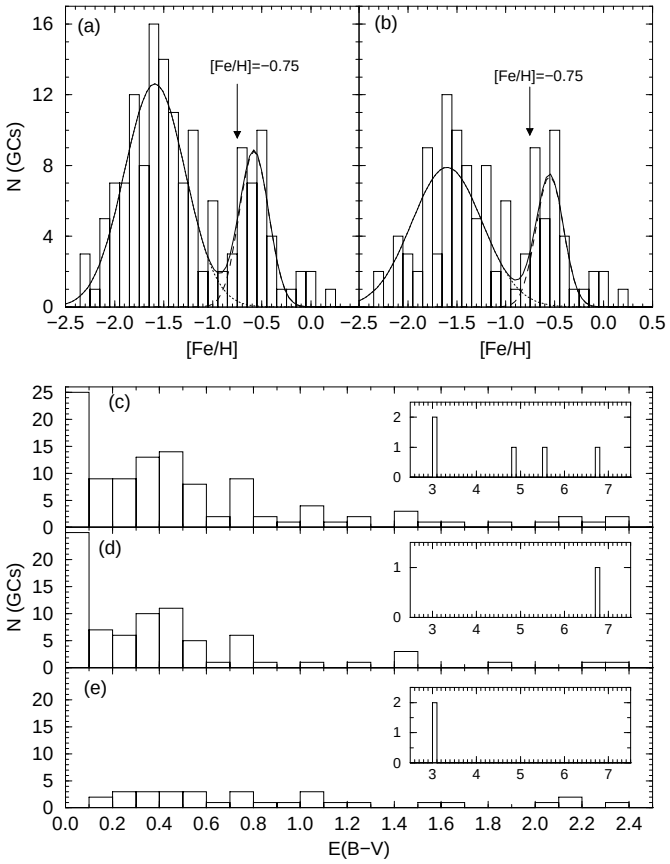

Fig. 1. GC metallicity distribution of the GC05 (panel (a)) and reduced samples (panel (b)). The adopted threshold between metal-rich and metal-poor GCs is indicated. The reddening distribution of the reduced sample GCs is in panel (c), the corresponding metal-poor ones are in panel (d) and the metal-rich ones in panel (e). The insets in panels (c) - (e) show the high-reddening range. Note that the two GCs with $E(B-V) \approx 4.8$ and 5.5 (inset of panel c) have no metallicity determinations.

a smaller one at $E(B-V) \approx 0.45$. The low-reddening values are related mostly to halo GCs, while the high-reddening ones belong to a more central metal-poor component that spatially coexists with the metal-rich bulge clusters (Barbuy, Bica & Ortolani 1998). The metal-rich GCs, in contrast, present a rather uniform distribution in the range $0.05 \leq E(B-V) \leq 1.3$.

3. Galactic structure and the distance to the center

Inferences on the geometry of the GC system can be made by means of cluster positions projected onto the (x,y,z)-heliocentric coordinate axes (Table 1). In this coordinate system the x-direction increases from the Sun towards the Galactic center, y is positive for $\ell = 0° - 180°$ and z increases towards the north Galactic pole. We consider separately the metal-rich and metal-poor GCs, both of the GC05 and RS-GC05 samples. In Fig. 2 we show the positions of the metal-rich GCs projected onto the (x,y), (x,z) and (y,z) planes for the GC05 (left panels) and RS-GC05 (right panels) samples. Because the (x,y,z) coordinates are in the heliocentric system, the centroids of the y and z distributions coincide with the Galactic center, while that of the x-coordinate is shifted from x = 0 (Sect. 3.1). GC05 metal-poor and metal-rich GCs are more widely distributed than those in RS-GC05. This effect is minimized in the RS-GC05 plots because most of the GC05 outliers belong e.g. to accreted dwarfs or their debris, have young ages and/or retrograde orbits (Table 1). The 2 remaining outliers in the metal-rich RS-GC05 (panels (b), (d) and (f)), NGC 6356 and Palomar 11, basically define the outer limits of the metal-rich system, slightly beyond the present determination of the Solar circle (see below) – 8 kpc (Reid 1993). These clusters deserve further attention to clarify whether they are young GCs, thus not related to the collapse, and/or located in the apogalacticon of their orbits.

From the plots involving the RS-GC05 sample (Fig. 2) we estimate that the metal-rich GCs distribute essentially in a region with dimensions $\Delta x \simeq 12$ kpc, $\Delta y \simeq 11$ kpc and $\Delta z \simeq 5$ kpc, corresponding to axial-ratios $\Delta x : \Delta y : \Delta z \approx 1.0 : 0.9 : 0.4$. These axial-ratios can be accounted for by an oblate spheroid with ~ 5.5 kpc in radius and ~ 2.5 kpc in height, a structure spatially coincident with the bulge. As compared to earlier studies the present x and y distributions of the metal-rich GCs are similar in extent (Fig. 2) because of the minimization of observational errors achieved with present-day data.

The metal-poor GCs of RS-GC05 are essentially contained in a region with dimensions $\Delta x \simeq 35$ kpc, $\Delta y \simeq 36$ kpc and $\Delta z \simeq 30$ kpc, with axial-ratios $\approx 1.0 : 1.0 : 0.8$. Considering uncertainties these axial ratios describe a slightly flattened sphere that reaches into the outer halo.

We also infer on the spatial distribution of the GCs in RS-GC05 by means of the distribution function $\phi(\xi) = \frac{dN}{d\xi}$, which counts the number of GCs in bins of $\Delta\xi = 1$ kpc, for the x, y and z coordinates. According to the definition, $\phi(\xi)$ is related to the projected one-dimensional number-density of GCs along a given direction. Fig. 4 shows the distribution functions of all GCs in RS-GC05, and the corresponding metal-poor and metal-rich ones, separately. As expected from Figs. 2 and 3, the distribution functions in y and z are symmetrical with respect to the centroid of the coordinate system (the Galactic center), while the shift in x provides the distance of the Sun to the Galactic center (Sect. 3.1). The distribution functions in Fig. 4 can be fitted both with exponential-decay and squared-hyperbolic secant functions. Exponential-decay functions usually describe projected surface-density profiles in spiral galaxy disks (Binney & Tremaine 1987), while self-gravitating isothermal models such as the squared-hyperbolic secant have been used in edge-on disks (e.g. Rice et al. 1996) and lenticular galaxies (van der Kruit & Searle 1981). Our purpose in fitting the distribution functions with a symmetrical profile is to derive the distance of the Sun to the

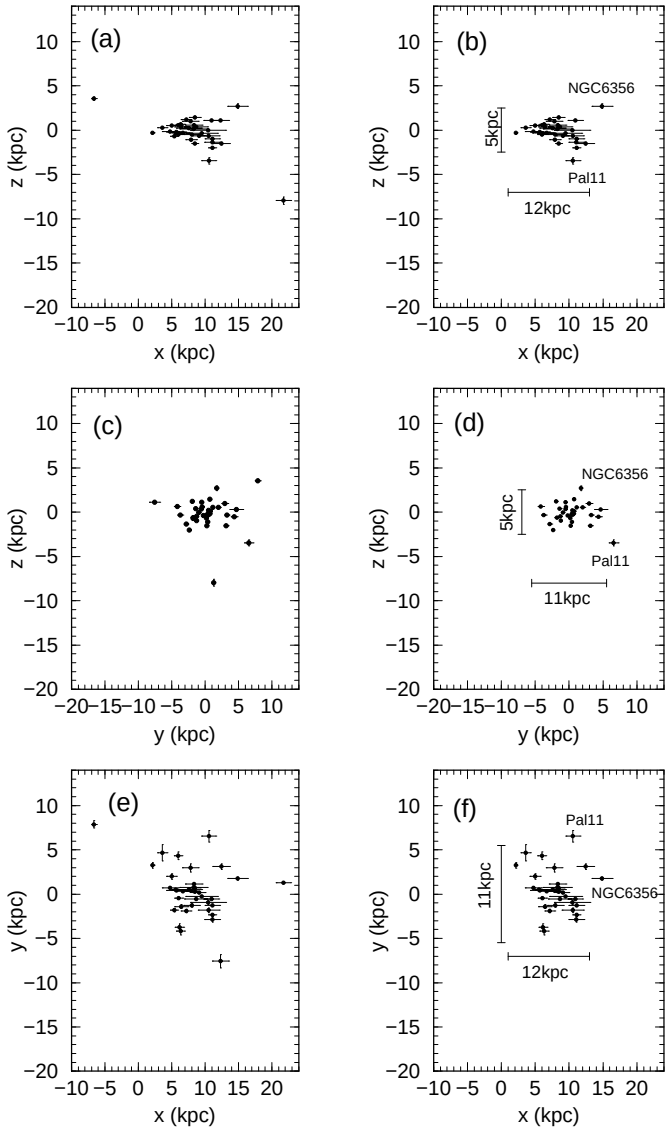

Fig. 2. Spatial projections of the heliocentric positions of the metal-rich GCs of the GC05 (left panels) and reduced (right panels) samples. The reduced sample produces more concentrated distributions. The outlier metal-rich GCs NGC 6356 and Palomar 11 are identified in panels (b), (d) and (f).

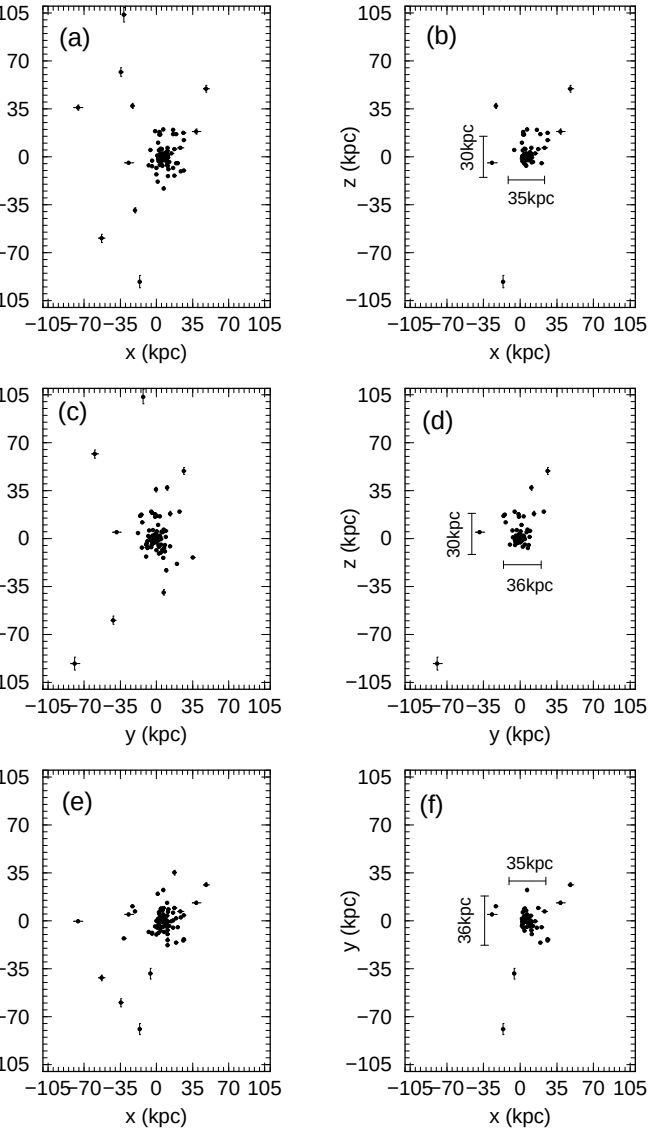

Fig. 3. Same as Fig. 2 for the metal-poor GCs.

Galactic center (Sect. 3.1). In this sense we adopted as fit the exponential-decay $\phi(\xi) \propto e^{-\left|\frac{\xi-\xi_o}{\xi_h}\right|}$ function, since the respective correlation coefficients resulted larger than with squared-hyperbolic secant functions. The fits are shown in Fig. 4, and the resulting central positions (ξ_o) and scale-lengths (ξ_h) are given in Table 2. The distribution peaks in y and z occur, within uncertainties, at y = z = 0 (Table 2 and Fig. 4).

Except for the central point in the y-distributions of the RS-GC05 sample (panel (b)) and corresponding metal-poor GCs (panel(e)) the exponential-decay function acceptably fits the observed data for distances of up to $\sim \pm 7$ kpc with respect to the peak, within uncertainties. At such distances we are probing not only the bulge but the inner halo as well. The fits preserve the symmetrical character of the observed profiles, and do not affect the centroid determination. This suggests that not many GCs remain undetected towards the central parts, at least to the point of affecting the distance determination.

The individual fit of an exponential-decay profile to each of the (x,y,z) components does not necessarily imply a disk structure for the GC subsystems, since we are dealing with one-dimensional distribution functions and not surface density profiles.

The scale-length ratios (Table 2) derived from the exponential-decay fits agree, within uncertainties, with the

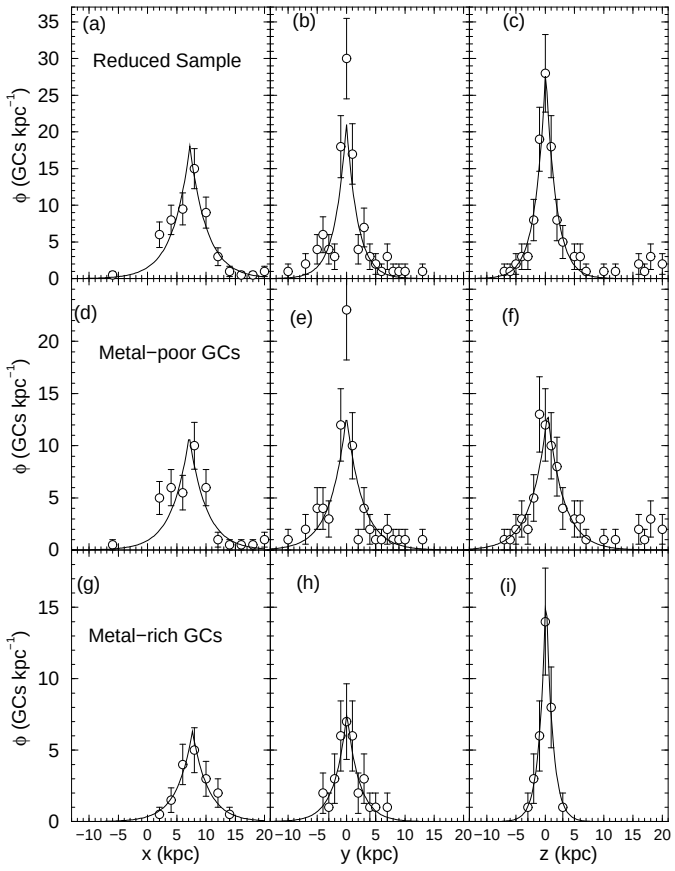

Fig. 4. One dimensional distribution functions of the reduced sample (top panels), metal-poor (middle panels) and metal-rich GCs (bottom panels). The profiles were fitted with the exponential-decay function $\phi(\xi) \propto e^{-\left|\frac{\xi-\xi_o}{\xi_h}\right|}$.

Table 2. Parameters of the one-dimensional distributions

	Reduced Sample GCs		
	All	Metal-Poor	Metal-Rich
(1)	(2)	(3)	(4)
x_o (kpc)	7.2 ± 0.3	7.1 ± 0.5	7.7 ± 0.3
x_h (kpc)	2.9 ± 0.4	2.9 ± 0.6	2.7 ± 0.4
y_o (kpc)	0.0 ± 0.3	0.0 ± 0.4	0.1 ± 0.3
y_h (kpc)	1.9 ± 0.4	2.8 ± 0.5	2.1 ± 0.4
z_o (kpc)	0.1 ± 0.2	0.4 ± 0.3	0.1 ± 0.1
z_h (kpc)	1.8 ± 0.2	2.7 ± 0.5	1.1 ± 0.1
x_h/y_h	1.5 ± 0.4	1.0 ± 0.3	1.3 ± 0.3
x_h/z_h	1.6 ± 0.3	1.1 ± 0.3	2.4 ± 0.4
y_h/z_h	1.1 ± 0.3	1.0 ± 0.2	1.9 ± 0.4

Table Notes. Parameters of the function $\phi(\xi) \propto e^{-\left|\frac{\xi-\xi_o}{\xi_h}\right|}$ fitted to the $\xi = (x, y, z)$ distribution functions. Col. (2): All GCs of the reduced sample.

axial-ratios estimated from Figs. 2 and 3, both for the metal-poor and metal-rich GCs of RS-GC05.

3.1. Distance to the Galactic center

The distance of the Sun to the Galactic center (R_O) has been a recurrent topic in the literature since Shapley's attempt in 1918 to derive it with globular clusters that resulted in $R_O = 13$ kpc. Since then different methods with more accurate data and larger GC samples have been used fot the same purpose. For instance Frenk & White (1982) using a sample of 65 metal-poor and 11 metal-rich GCs limited in latitude to avoid exceedingly large reddening errors affecting distances derived $R_O = 6.8 \pm 0.8$ kpc.

Reid (1993) reviewed several estimators to derive R_O, among them the available GC parameters at that time. Estimates based on those GCs put R_O in the range 6.2–10.1 kpc. The average R_O from the GC determinations in Table 2 of Reid (1993) is 7.9 ± 1.4 kpc, which coincides with his best value of 8.0 ± 0.5 kpc considering all methods, e.g. calibration by OB stars and H I and H II regions, GCs, RR Lyrae and red giants, among others. Since then this value has been widely employed in the literature. However, from his Fig. 3 it is clear that the x coordinates of the available GCs suffer from reddening/distance uncertainty effects. With the GC samples available at the time Maciel (1993) and Rastorguev et al. (1994) obtained $R_O \approx 7.6$ kpc and $R_O \approx 7.0$ kpc, respectively.

More recently, Eisenhauer et al. (2003) used VLT spectroscopic observations of the orbit of the star S2 around SgrA* (assumed to be at the very center of the Galaxy) to derive $R_O = 8.0 \pm 0.4$ kpc. In the same work they provide as well the value of R_O based on the statistical parallax distance of 106 late-type and 27 early-type stars located in the central 0.5 pc. They obtained $R_O = 7.2 \pm 0.9$ kpc.

One caveat is that the total-to-selective absorption ratio $R_V = A_V/E(B-V)$ is not expected to be uniform. Variations of R_V in different directions throughout the Galaxy can occur (e.g. Sumi 2004; Ducati, Ribeiro & Rembold 2003). R_V is also affected by the effective wavelength shift in the filters owing to metallicity differences and reddening amount (Barbuy, Bica & Ortolani 1998, and references therein). Detailed analyses of R_V in the directions of all GCs would be necessary to minimize R_V-related uncertainties. However, to a first approximation we assumed the H03 distances in Table 1. H03 took into account the metallicity dependence of the absolute magnitude of the horizontal branch and from their data it can be inferred that a constant value of $R_V = 3.1$ was adopted throughout.

At the 1σ level the values of R_O provided by the one-dimensional exponential-decay fits of the metal-poor (panel (d) of Fig. 4) and metal-rich GCs (panel (g)) are basically the same (Table 2). In this sense, to increase the statistical significance of the determination we applied the fit to the 116 GCs of RS-GC05 (panel (a) of Fig. 4). We obtained an average value of $R_O = 7.2 \pm 0.3$ kpc. This value puts the Sun ≈ 0.8 kpc closer to the Galactic center than either the best one adopted by Reid (1993) or that derived by Eisenhauer et al. (2003). However, the present

value coincides with that of central stars by Eisenhauer et al. (2003).

The present determination is based on a more accurate and numerous GC database, and consequently, the uncertainties in the value of R_O are a factor of ~ 3 smaller than in previous studies using GCs (see Table 2 of Reid 1993). We used the new R_O determination to recalculate the Galactocentric distances (col. 8 of Table 1).

3.1.1. Variable total-to-selective absorption

Following the analysis of Barbuy, Bica & Ortolani (1998) of the central Galaxy, we now explore the effect of a varying total-to-selective absorption as a function of metallicity and reddening amount for the whole GC system. According to Grebel & Roberts (1995) we adopted $R_V = 3.6$ for the GCs more metal-rich than solar metallicity, and $R_V = 3.1$ for [Fe/H] ≤ -1.0. Interpolation is used for intermediate values of metallicity. To the metallicity-interpolated R_V we add a further correction related to reddening, $\Delta R_V = 0.05 \times E(B-V)$ (Olson 1975). Dependence of distance on varying R_V can be expressed as $Ro' = Ro \times 10^{\frac{(R_V - R'_V)E(B-V)}{5}}$.

We applied the above corrections to the data in Table 1 for all metal-rich GCs of RS-GC05 individually, leading to a smaller value of $Ro = 6.6 \pm 0.5$ kpc. Applying the same to all metal-poor GCs of RS-GC05 individually the distance of the Sun to the Galactic center remains essentially the same as before $Ro = 7.3 \pm 0.5$ kpc (Table 2).

Finally, we consider the ensemble of the metal-rich GCs (Fig. 1) in order to minimize individual uncertainties. The average metallicity and reddening are [Fe/H] ≈ -0.55 and $E(B-V) \approx 0.5$, providing an average $R'_V = 3.35$. For the metal-rich GCs $R_V = 3.1$ (Sect. 3.1) and $Ro = 7.7 \pm 0.5$ kpc (Table 2), and the resulting distance is $Ro' = 7.3 \pm 0.3$ kpc, thus fully compatible with Ro derived from the metal-poor GCs.

Irrespective of the metallicity and reddening law variations for the metal-rich GCs, the present distance of the Sun to the Galactic center determination $Ro \approx 7.2$ kpc is robust, since it depends essentially on the larger sample of metal-poor GCs. This is due to the metal-poor GCs being rather insensitive to R_V assumptions and the fact that the current accuracy on their distances is significantly improved.

4. Radial distribution of globular clusters

The distribution in Galactocentric distance of the GC number-density, $\rho(R) = \frac{dN}{dV} = \frac{dN}{4\pi R^2 dR}$, is a potential source of information not only on the present-day Galactic structure but the formation processes as well. To investigate this we build radial distribution profiles for the metal-rich and metal-poor GCs of RS-GC05 separately. Bins in radius of $\Delta R = 0.5$ kpc for $R_{GC} \leq 10$ kpc are used to better sample the inner regions, while $\Delta R = 2$ kpc for $10 \leq R_{GC}(kpc) \leq 20$ and $\Delta R = 10$ kpc for $R_{GC} \geq 20$ kpc to avoid undersampling with increasing Galactocentric distance. Taken as face value the radial distribution function as defined above should be applied to spherically symmetric systems, which is not the case of the oblate geometry of the metal-rich GCs of RS-GC05 (Sect. 3). Implications of this difference in geometry will be discussed in Sect. 4.4.

4.1. Metal-poor GCs

The radial distribution of the metal-poor GCs of RS-GC05 is shown in panel (a) of Fig. 5. A fraction of 74% of the 81 metal-poor GCs is located at Galactocentric distances $R_{GC} \leq 10$ kpc, and 20% at $R_{GC} \geq 15$ kpc (outer halo). The distribution falls off smoothly as a rather steep power-law $\sim R^{-(3.6 \pm 0.2)}$ for $R_{GC} \geq 3.5$ kpc. However, it flattens out for smaller Galactocentric distances as $\sim R^{-(1.7 \pm 0.3)}$. At least part of the flattening might be attributed to completeness effects in the crowded central region of the Galaxy. However, a near-IR survey with 2MASS (Dutra & Bica 2000) did not reveal any new GC in the central region. Two recent GC discoveries with 2MASS are not centrally located, since they are at $l \approx 10^\circ$ and near the plane, about halfway from the Sun to the Galactic center (Hurt et al. 2000). Alternatively, the flattening for small R_{GC} may result from the cumulative destruction of GCs close to the Galactic center over a Hubble time (a process that certainly played a major rôle in depleting the original GC population - see Sect. 4.5), or it may be an intrinsic feature of the radial distribution. Modelling of the spatial distribution of the old halo GCs beginning at the primordial collapse with cold baryonic gas and dark matter conditions suggests that the inner flattening may result not only from tidal destruction, but may in part be of primordial origin (Parmentier & Grebel 2005).

Because of the flattening at small R_{GC} the simplest fits of the observed radial density profile are obtained with analytical functions that contain a core-like term. Following Djorgovski & Meylan (1994) we employ the function $\rho(R) = \rho_o/(1 + R/R_C)^\alpha$, where R_C is the core-like radius. We will refer to this function as the composed power-law. The agreement between fit and observed radial distribution along the full Galactocentric distance range is excellent (Fig. 5, panel (a)). The resulting parameters are $\rho_o = 3.9 \pm 2.5$ kpc^{-3}, $R_C = 1.5 \pm 0.6$ kpc and $\alpha = 3.9 \pm 0.3$, with a correlation coefficient CC = 0.88.

Alternatively, in the inset of panel (a) we fit the metal-poor observed radial profile with Sérsic's (1966) law, $\rho(R) = a\, e^{-b\left[(R/R_C)^{(1/n)} - 1\right]}$. Since it is rather insensitive to variations of R_C, we used the same core-like radius as that indicated by the composed power-law in order to have less free parameters when fitting Sérsic's law. The best fit was obtained with $n = 4.1 \pm 0.7$ and CC = 0.88.

4.2. Metal-rich GCs

The 33 metal-rich GCs of RS-GC05 are contained in the region $0.66 \leq R_{GC}(kpc) \leq 8.3$ (panel (b)), which shows that a sharp radial cutoff thus occurs in the metal-rich distribution near the Solar circle. Metal-rich GCs in GC05 located outside this region appear to be related to accretion of dwarfs and/or young ages (Table 1). This contrasts with the metal-poor GCs that distribute in the range $0.36 \leq R_{GC}(kpc) \leq 123$. Similarly to the metal-poor GCs, a flattening in the radial distribution of the metal-rich GCs with respect to the extrapolation of the large Galactocentric distance power-law $\sim R^{-(3.2\pm0.2)}$ occurs for $R_{GC} \leq 2\,kpc$. This effect should be expected, since there is a lack of correlation of metallicity and GC luminosity (e.g. Djorgovski & Meylan 1994; van den Bergh 2003). Parameters of the composed power-law fit are $\rho_o = 6.3 \pm 5.2\,kpc^{-3}$, $R_C = 1.2 \pm 1.0\,kpc$ and $\alpha = 3.9 \pm 1.2$, with CC = 0.88. Sérsic's law (inset of panel (b)) provides a fit with the exponent $n = 2.9 \pm 1.5$ (CC = 0.87). In this fit we used $R_C = 1.2 \pm 1.0\,kpc$, as indicated by the composed power-law. The observed distribution (panel (b) of Fig. 5) cannot be fitted with an exponential-decay law, which precludes the presence of a disk.

Probably as a consequence of the bulge/halo transition, the flattening in both metal-poor and metal-rich radial distributions begin at Galactocentric distances compatible with the dimension of the bulge (Sect. 3), particularly with the (x,y,z) scale-lengths of the metal-rich GCs (Table 2).

Despite the marked difference in the radial extent of the metal-rich and metal-poor GC profiles, both distributions present similar structural features such as flattening in the central region, core-like radius ($R_C = 1.2-1.5\,kpc$), composed ($\alpha = 3.9$) and single power-law slopes ($n = 3.2 - 3.5$) and Sérsic's law index ($n = 2.9 - 4.1$), within uncertainties. These similarities suggest that most of the GCs in both metallicity classes share a common origin.

4.3. All GCs of the reduced sample

The best-fit of the composed power-law to the radial distribution of the 116 RS-GC05 GCs was obtained with $\rho_o = 7.2 \pm 3.0\,kpc^{-3}$, $R_C = 1.9 \pm 0.5\,kpc$ and $\alpha = 4.4 \pm 0.3$, with CC = 0.91 (panel (c) of Fig. 5). Because the metal-rich GCs are contained in the region $R_{GC}(kpc) \leq 8.3$ the slope of the composed power-law resulted slightly steeper than those of the metal-rich and metal-poor distributions, as expected. In addition, the single power-law extrapolation for $R_{GC} \geq 3.5\,kpc$ falls off as $\sim R^{-(3.9\pm0.1)}$, which within uncertainties basically agrees with that of the metal-poor GCs. The best Sérsic's law fit was obtained with $n = 3.0 \pm 0.4$ and CC = 0.89. Qualitatively, Sérsic's law and the composed power-law provide essentially the same fit to the observed radial profile.

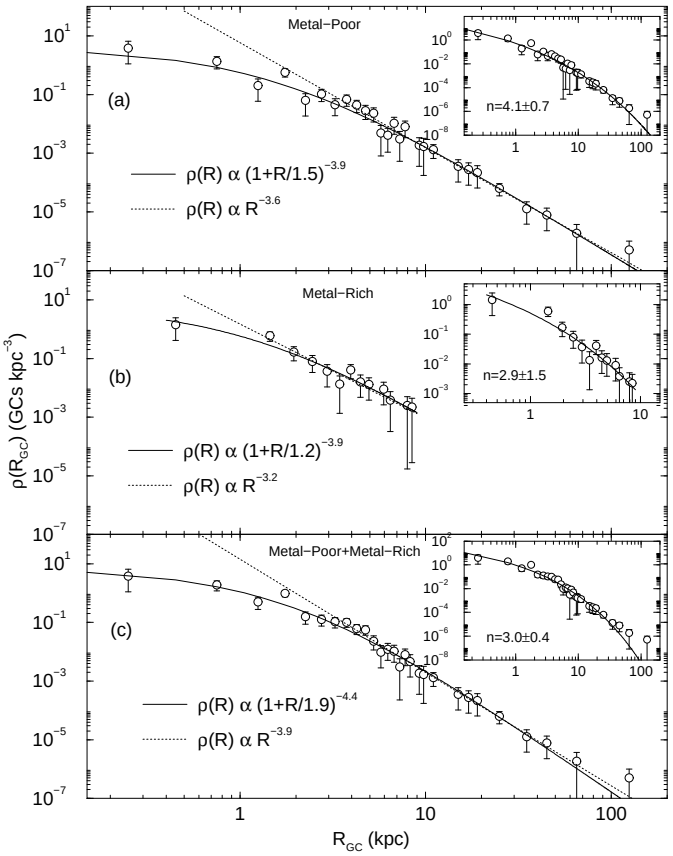

Fig. 5. Radial density profiles of the GCs in the reduced sample as a function of Galactocentric distance. Panel (a) - metal-poor GCs; Panel (b) - metal-rich; Panel (c) - all GCs. Dashed line: single power-law fit for large Galactocentric distances. Solid line: fit of $\rho(R) = \rho_o/(1 + R/R_C)^\alpha$. Insets: fit of Sérsic's law $\rho(R) = a\,e^{-b\left[(R/R_C)^{(1/n)}-1\right]}$.

4.4. Spherically symmetric-volume densities for the oblate metal-rich sub-system

For practical purposes we assumed spherical symmetry in the above analysis of metal-rich and metal-poor radial density profiles. However, the metal-rich GCs distribute through a region whose geometry is clearly oblate (Sect. 3). Thus, spherically symmetric-volume densities calculated in radial bins beyond a few kpc from the center will be artificially decreased, as compared to those measured in a genuinely (or approximately) spherical system. Consequently, both the measured power-law fall-off at large radii and central flattening degree in the metal-rich sub-system might result enhanced relative to the nearly spherically symmetric metal-poor sub-system.

To investigate the effects of non-sphericity in the metal-rich sub-system we apply a coordinate transformation to correct for its oblateness, $y \rightarrow y/0.9$ and $z \rightarrow z/0.4$ (Sect. 3). Subsequently we recalculate Galactocentric distances, $R_{GC} = \sqrt{x^2 + y^2 + z^2}$, and volume densities, $\rho(R)$. Compared to the observed oblate profile (bottom panel) the corrected one (top panel of Fig. 6) presents

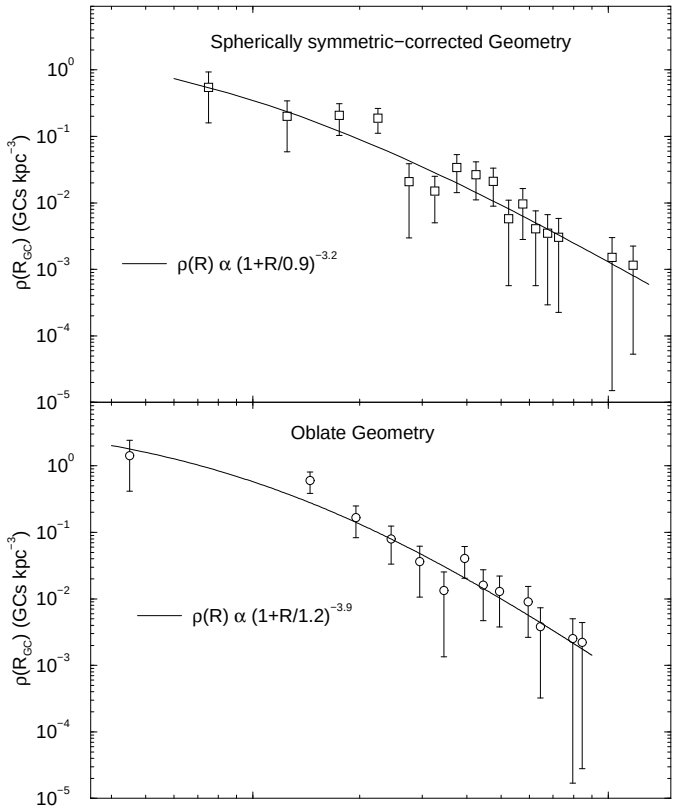

Fig. 6. Radial density profiles of the metal-rich GCs in the reduced sample measured with spherically symmetric volume densities on oblateness-corrected (top panel) and oblate (bottom panel) spatial geometries.

similar shape and somewhat scaled-up Galactocentric distances. Fit of the composed power-law results in a core-like $R_C = 0.9 \pm 0.9$ kpc and slope $\alpha = 3.2 \pm 0.9$. Both R_C and α are similar to the previous ones, but the slope is somewhat flatter, as expected.

Within uncertainties we conclude that measuring spherically symmetric volume densities in the oblate metal-rich GC sub-system has a small effect on structural parameters such as power-law fall-off at large radii and flattening degree in the central region. The effect is minimal probably because of the relatively small radial extension ($R_{GC} \sim 10$ kpc) of the metal-rich sub-system. This effect is negligible for the nearly-spherical metal-poor GC sub-system (Sect. 3).

4.5. Globular cluster destruction rates

The discussions in the previous section raised the question whether the flattening observed in the radial distribution for regions interior to $R_{GC} \sim 2$ kpc is a primordial feature or a consequence of enhanced GC-destruction rates near the Galactic center. Although the present analysis does not answer this question, it can be used to provide an estimate on the fraction of primordial GCs still present in the Galaxy.

The Galactic environment, particularly near the center, tends to destroy star clusters because of enhanced tidal truncation and gravitational shocks due to passages close to the bulge and through the disk. The bulge, in particular, is very efficient in destroying clusters on highly elongated orbits (Gnedin & Ostriker 1997), and the presence of the bar increases the destruction rates by providing a means to bring more clusters close to the Galactic center (Long, Ostriker & Aguilar 1992). Dynamical evaporation is probably the most important destruction mechanism in the present-day Galactic environment (Gnedin & Ostriker 1997). Aguilar, Hut & Ostriker (1988) estimate a current GC depletion rate of $\sim 5\%$ due basically to dynamical evaporation, indicating that most of the destruction took place in the past with bulge-shocking as the main factor. Hut & Djorgovski (1992) estimate that the present GC evaporation rate may be $5 \pm 3\,\mathrm{Gyr}^{-1}$.

Gnedin & Ostriker (1997) found larger destruction rates than previous work, predicting that 52% – 86% of the present GC population may be destroyed in the next Hubble time. They conclude that the present GC population must be a small fraction of the primordial one, with the debris of the destroyed clusters constituting a large fraction of the spheroidal (bulge + halo) stellar population. Mackey & van den Bergh (2005) by means of observational differences in properties of three Galactic GC subsystems estimate that the present population could be a fraction $\sim 2/3$ of the original one. Mackey & Gilmore (2004) estimate a lower limit of 50% for the destruction rate over the last Hubble time, an intermediate value between those of Gnedin & Ostriker (1997) and Mackey & van den Bergh (2005).

At large Galactocentric distances the efficiency of the GC destruction mechanisms should be minimized with respect to the central region. This assumption is supported by numerical simulations showing that low-concentration, high-mass GCs are efficiently destroyed in the inner halo but are able to survive at $R_{GC} \geq 10$ kpc (Vesperini & Heggie 1997). For large R_{GC} the number-density of GCs in RS-GC05 is well described by the single power-law $\rho(R) = (14.2 \pm 3.3) R^{-(3.9 \pm 0.1)}$, the discrepancy with respect to the observed profile becoming increasingly larger for $R_{GC} \leq 3$ kpc (Fig. 5 - panel (c)).

An estimate of the past destruction rate can be derived by comparing the number of GCs in RS-GC05 with that corresponding to the extrapolation of the large-R_{GC} power-law to the inner regions, under the assumption that the difference in both numbers is basically due to the cumulative past destruction of GCs. This estimate should be taken as lower-limit since we neglect GC destruction for large R_{GC}. To derive this value we integrate the large-R_{GC} power-law through the Galactocentric distance range over which the 116 GCs of RS-GC05 are observed. Taking into account the uncertainties in the parameters of the power-law fit we estimate that the present GC population represents a fraction of $\leq 23 \pm 6\%$ of the primordial one. Thus, a lower-limit for the past destruction rate is $\sim 77\%$ over a Hubble time. This estimate is compatible with that

in Gnedin & Ostriker (1997) and about three times larger than that derived by Mackey & van den Bergh (2005).

The above estimate is based on the assumption that the flattening in the central radial profile is essentially due to GC destruction. However, if the flattening is partly primordial, as suggested by Parmentier & Grebel (2005), the $\sim 77\%$ destruction rate should in fact be taken as an approximate upper limit. In this case our estimate would agree with the central range of Gnedin & Ostriker (1997).

4.6. The central kpc

With the present determination of the Galactocentric distance (Sect. 3.1), 9 GCs of the reduced sample are located within 1 kpc of the Galactic center (H03 contains 11 such GCs). The metal-poor GCs are Palomar 6 and HP 1 at $R_{GC} \leq 0.5$ kpc, and NGC 6355, Terzan 9, NGC 6522, NGC 6558, and NGC 6401 at $0.5 \leq R_{GC}(\mathrm{kpc}) \leq 1.0$. The metal-rich ones are Terzan 5 and ESO 456 SC38 at $0.6 \leq R_{GC}(\mathrm{kpc}) \leq 0.7$. Errors affect these individual estimates, but the ensemble might give hints on the extent of a potential avoidance zone, or a central region of enhanced destruction rates (e.g. Aguilar, Hut & Ostriker 1988).

5. Discussion

In the analysis of the reduced sample GCs we found that the radial density profiles of the metal-rich and metal-poor GCs are well described by a composed power-law of the form $\rho(R) \propto (1 + R/R_C)^{-\alpha}$, with $3.9 \leq \alpha \leq 4.4$. For Galactocentric distances larger than ~ 2 kpc both observed profiles fall off as a single power-law R^{-n} with $3.2 \leq n \leq 3.9$, while for inner regions they both flatten in a similar way. Structurally, the only difference besides geometry (Sect. 3) between the spatial distributions of the metal-rich and metal-poor GCs is that the former extends basically to the Solar circle, while the latter spans from the central parts to the outer halo. This suggests that a significant fraction of the metal-rich and metal-poor GCs share a common origin. These conclusions are not significantly affected by the oblate and nearly spherical geometries of the metal-rich and metal-poor sub-systems, respectively (Sect. 4.4).

As pointed out by Djorgovski & Meylan (1994), the analytical function that we adopted to fit the radial density profiles does not have a physically consistent counterpart. However, the steep slopes implied by this function for the GC radial density profiles rule out scenarios involving the pure monolithic collapse of an isothermal, uniform density cloud. This kind of collapse would produce flatter radial density profiles (Abadi, Navarro & Steinmetz 2005, and references therein). In addition, RS-GC05 radial density slopes are significantly steeper than that of the dark matter halo (Merritt et al. 2005), which in principle precludes a common origin of these structures. Consequently, additional mechanisms might have been necessary to increase the density of GCs in the central regions of the Milky Way, such as mergers in the early phases.

The rather steep density distribution of the stellar halo was previously derived using globular clusters, RR Lyrae stars, blue horizontal-branch (BHB) stars, and star counts. Harris (1976) and Zinn (1985) have shown that the metal-poor GCs distribute radially following a R^{-n} power-law profile, with $n = 3.5$. Using observations of RR Lyrae Hawkins (1984) derived $n = 3.1$ with an axial ratio $c/a = 0.9$. Bahcall & Soneira (1984) and Gilmore (1984) found $c/a \approx 0.8$. Using BHB stars Preston, Shectman & Beers (1991) found an increase in the axial ratio from $c/a \approx 0.5$ to $c/a \approx 1$ up to 20 kpc with $n = 3.5$. Recently, Yanny et al. (2000) used BHB tracers from Sloan Digital Sky Survey data to derive $c/a = 0.65$ and $n = 3.2$. Ivezić et al. (2000) found that the RR Lyrae column density follows a shallower power law with $n = 2.7$. Robin, Reylé & Crézé (2000) from deep wide field star counts estimated a halo flattening of 0.76, and $n = 2.44$.

Evidence of merger events in galaxies has considerably increased in recent years, both on observational and theoretical grounds. Deep observations of stars in luminous halos associated with numerical simulations of galaxy formation in Λ-cold dark matter (ΛCDM) scenarios indicate that a large fraction of the stellar content in the halo was not formed *in situ*. Abadi, Navarro & Steinmetz (2005 and references therein) suggest that this fraction may have been accreted from protogalaxies during earlier merger events. The resulting mass density profiles behave as a power-law R^{-n} with $n = 3$ at the luminous edge of the galaxy and $n \geq 4$ more externally, at the virial radius. In addition, the density profile of the outer stellar halo is more centrally concentrated with a steeper slope than the dark matter halo, whose density profile is caracterized by slopes $n = 1 - 3$ (Merritt et al. 2005). Hierarchical galaxy formation models under the ΛCDM framework that are successful in reproducing the radial density profile of the Milky Way stellar halo indicate that this structure formed from ~ 100 tidally disrupted, accreted dwarf satellites (Bullock, Kravtsov & Weinberg 2001). What emerges from this is an observational/theoretical picture for the formation and evolution of the stellar halo involving violent relaxation and accretion, consistent with hierarchical models of galaxy formation (Bellazzini, Ferraro & Ibata 2003; Abadi, Navarro & Steinmetz 2005).

In this sense, the observed similarity of the metal-rich and metal-poor radial density profiles of the Galactic GC system with that of the stellar halo suggests that, in addition to the GCs formed in the primordial collapse, a non-negligible fraction of the GCs presently in the Milky Way was probably accreted during an early period of active merging. This scenario seems to apply to the bulge as well, which raises the possiblity of an early merger affecting the central parts of the Galaxy. In the present universe there are examples of such mergers, e.g. NGC 1275 (Zepf et al. 1995; Holtzman et al. 1992).

Additional support for this scenario comes from the fact that the radial density profiles of the GCs of the reduced sample are equally well fitted by Sérsic's law,

$\rho(R) \propto e^{-b[(R/R_C)^{(1/n)}-1]}$, with n $\approx$ 4.1 (metal-poor), n $\approx$ 2.9 (metal-rich), and n $\approx$ 3.0 (combined metal-poor/metal-rich GCs). Sérsic's law with $2 \leq n \leq 4$ is thought to apply to systems resulting from the mixing that follows from violent relaxation or merging (Merritt et al. 2005, and references therein). Besides, chemical evolution models that reproduce the observed abundances of stars in the bulge suggest that the Galactic bulge formed from the same gas but faster than the inner Galactic halo (Matteucci & Romano 1999; Matteucci, Romano & Molaro 1999). The minimum at about [Fe/H] ≈ -0.75 in the observed metallicity distribution of GCs (Fig. 1) may reflect an external mechanism such as merging to explain the exceedingly large number of metal-rich GCs. An early merger in the Milky Way with a relatively massive galaxy might have provided the excess metal-rich star formation in the central parts.

Further evidence on the bulge formation via collapse and/or additional mechanisms will be given by detailed derivation of metallicities and abundance ratios in comprehensive samples of GCs. However, such detailed information for bulge GCs is presently scarce.

6. Concluding remarks

In this paper the Galactic globular cluster system was decontaminated of the objects with strong evidence of external origin and/or ages younger than the Galaxy collapse. The resulting reduced sample contains 116 GCs, 81 metal-poor and intermediate metallicity clusters ([Fe/H] ≤ -0.75), 33 metal-rich and 2 with unknown metallicity. The classical bimodal metallicity distribution is enhanced in the reduced sample.

Projections of the observed heliocentric distances onto the (x,y,z) planes show that the metal-rich GCs distribute in a central region of dimensions $\sim 12\,\mathrm{kpc} \times 11\,\mathrm{kpc} \times 5\,\mathrm{kpc}$, whose structure resembles an oblate spheroidal with axial ratio c/a ≈ 0.4. The metal-poor ones span a region of dimensions $\sim 35\,\mathrm{kpc} \times 36\,\mathrm{kpc} \times 30\,\mathrm{kpc}$, with a shape similar to a slightly flattened sphere with c/a ≈ 0.8. The metal-poor GCs in the reduced sample extend into the beginning of the outer halo. Based on the projected number-density of GCs along the x-direction we measured the distance of the Sun to the Galactic center as $R_O = 7.2 \pm 0.3\,\mathrm{kpc}$. This value was obtained considering the spatial distribution of 116 GCs, and is $\sim 10\%$ smaller than the widely used estimate of Reid (1993).

Based on structural similarities of the radial density profiles of the present-day GC population with the stellar halo one can build a scenario where, besides the GCs formed in the primordial collapse, a non-negligible fraction of the Milky Way GCs was probably accreted from satellites during an early period of merging. Observational and theoretical evidence support this picture, e.g. the GCs formed as a consequence of mergers in NGC 1275 (Zepf et al. 1995; Holtzman et al. 1992).

The present decontamination procedure was not sensitive to all accretions that may have occurred in the first Gyrs of the Galaxy, including an eventual major merging, since the observed radial density profiles still appear to preserve traces of the earliest merger(s).

Assuming that the flattening in the observed radial density profiles is a consequence of the cumulative GC depletion mostly by bulge and disk shocking we estimated that the present GC population represents a fraction of $\leq 23 \pm 6\%$ of the original one. This in turn implies a lower-limit destruction rate of $\sim 77\%$ over a Hubble time. This estimate is compatible with that of Gnedin & Ostriker (1997) and somewhat larger than that derived by Mackey & van den Bergh (2005). However, if the central flattening is partly primordial (Parmentier & Grebel 2005) our estimate would in fact be an upper limit.

The significant improvement in the accuracy of GC data over the last years, as analysed in the present work, has shed light on the issue whether the metal-rich GCs are associated to a disk (e.g. Zinn 1985; Armandroff 1989) or a spheroidal subsystem. The fact that the volume-density radial distribution of GCs of the reduced sample can be described both by a core-like power-law or a Sérsic's law indicates that the metal-rich GC subsytem is spheroidal.

The present study pointed out that besides the GC accretions from dwarfs and/or formation later than the primordial collapse, the radial density distributions require, in addition to a primordial collapse component a non-negligible early merger population. This scenario provides also a natural explanation to the second peak in the bimodal metallicity distribution. Through gravitational lensing, large galaxies at high-redshift have been detected in the starburst stage, in an epoch compatible to that of the Milky Way's primordial collapse. Examples are the z $\sim$ 7 and M $\sim 10^9\,M_\odot$ galaxy lensed by the Abell 2218 cluster (Egami et al. 2005), and the z $\sim$ 5.5, $M \sim 1-6 \times 10^{10}\,M_\odot$ starforming galaxy in the field of the cluster RDCS 1252.9-2927 (Dow-Hygelund et al. 2005). Collapse or its combination with merging are supported by the Galactic GCs and large redshift observations of galaxies. On the other hand pure hierarchical galaxy formation has yet to be observed in detail.

Acknowledgements. E.B., C.B. and B.B. acknowledge support from the Brazilian Institution CNPq. S.O. acknowledges support from Ministero dell'Università e della Ricerca Scientifica e Tecnologica (MURST) under the program on 'Fasi Iniziali di Evoluzione dell'Alone e del Bulge Galattico' (Italy). We thank an anonymous referee for comments.

References

Abadi, M.G., Navarro, J.F. & Steinmetz, M. 2005, MNRAS, submitted (astro-ph/0506659)
Aguilar, L., Hut, P. & Ostriker, J.P. 1988, ApJ, 335, 720
Armandroff, T.E. 1989, AJ, 97, 375
Bahcall, J.N. & Soneira, R.M. 1984, ApJS, 55, 67
Barbuy, B., Ortolani, S., Bica, E. & Desidera, S. 1999, AJ, 348, 783
Barbuy, B., Bica, E. & Ortolani, S. 1998, A&A, 333, 117
Bellazzini, M., Ferraro, F. & Ibata, R. 2003, AJ, 125, 188

van den Bergh, S. 1993, AJ, 105, 971
van den Bergh, S. 2000, in *The Galaxies of the Local Group*, (Cambridge: Cambridge University Press), UK, Cambridge Astrophysics Series Series, vol no: 35
van den Bergh, S. 2003, ApJ, 590, 797
Binney, J. & Tremaine, S. 1987, in *Galactic Dynamics*, Princeton, NJ: Princeton University Press. (Princeton series in astrophysics)
Bullock, J.S., Kravtsov, A.V. & Weinberg, D.H. 2001, ApJ, 548, 33
Carraro, G. 2005, ApJ, 621, 61
da Costa, G.S. & Armandroff, T.E. 1995, AJ, 109, 2533
Coté, P., Welch, D.L., Fischer, P. & Gebhardt, K. 1995, ApJ, 454, 788
Coté, P. 1999, AJ, 188, 406
Dinescu, D.I., Girard, T.M. & van Altena, W.F. 1999, AJ, 117, 1792
Djorgovski, S. & Meylan, G. 1994, AJ, 108, 1292
Dow-Hygelund, C.C., Holden, B.P., Bouwens, R.J. et al. 2005, ApJL, 630, 137
Ducati, J.R., Ribeiro, D. & Rembold, S.B. 2003, ApJ, 588, 344
Dutra, C.M. & Bica, E. 2000, A&A, 359, 9
Egami, E., Kneib, J.-P., Rieke, G. H. et al. 2005, ApJL, 618, 5
Eggen, O.J., Lynden-Bell, D. & Sandage, A.R. 1962, ApJ, 136, 748
Eisenhauer, F., Schödel, R., Genzel, R., Ott, T., Tecza, M., Abuter, R., Eckart, A. & Alexander, T. 2003, ApJL, 597, 121
Forbes, D.A., Strader, J. & Brodie, J.P. 2004, AJ, 127, 3394
Frenk, C.S. & White, S.D.M. 1982, MNRAS, 198, 173
Gilmore, G. 1984, MNRAS, 207, 223
Gnedin, O.Y. & Ostriker, J.P. 1997, ApJ, 474, 223
Grebel, A.K. & Roberts, W. 1995, A&AS, 109, 293
Guo, X., Girard, T.M., van Altena, W.F. & Lopez, C.E. 1993, AJ, 105, 2182
Harris, W.E. 1976, AJ, 81, 1095
Harris, W.E. 1996, AJ, 112, 1487
Harris, W.E., Phelps, R.L., Madore, B.F., Pevunova, O. & Skiff, B.A. 1997, AJ, 113, 688
Hawkins, M.R.S. 1984, MNRAS, 206, 433
Holtzman, J.A., Faber, S.M., Shaya, E.J. et al. 1992, AJ, 103, 691
Hurt, R.L., Jarrett, T.H., Kirkpatrick, J.D., et al. 2000, AJ, 120, 1876
Hut, P. & Djorgovski, S. 1992, Nature, 359, 806
Ibata, R.A., Irwin, M.J. & Gilmore, G. 1994, Nature, 370, 194
Ibata, R.A., Wyse, R.F.G., Gilmore, G., Irwin, M.J. & Suntzeff, N.B. 1997, AJ, 113, 634
Ivezić, Z., Goldston, J., Finlator, K. et al. 2000, AJ, 120, 963
Kinman, T.D. 1959, MNRAS, 119, 538
Kobulnicky, H.A., Monson, A.J., Bickalew, B.A. et al. 2005, AJ, 129, 239
van der Kruit, P.C. & Searle, L. 1981, A&A, 105, 115
Long, K., Ostriker, J.P. & Aguilar, L. 1992, ApJ, 388, 362
Maciel, W.J. 1993, ApSS, 206, 285
Mackey, A.D. & van den Bergh, S. 2005, MNRAS, 360, 631
Mackey, A.D. & Gilmore, G.F. 2004, MNRAS, 355, 504
Matteucci, F. & Romano, D. 1999, Ap&SS, 265, 311
Matteucci, F., Romano, D. & Molaro, P. 1999, A&A, 341, 458
Merritt, D., Navarro, J., Ludlow, A. & Jenkins, A. 2005, ApJL, 624, 85
Minniti, D. 1995, AJ, 109, 1663
Olson, B.I. 1975, PASP, 87, 349
Ortolani, S., Bica, E. & Barbuy, B. 2000, A&A, 361, L57
Parmentier, G. & Grebel, E.K. 2005, MNRAS, 359, 615
Phelps, R.L. & Schick, M. 2003, AJ, 126, 265
Preston, G.W., Shectman, S.A. & Beers, T.C. 1991, ApJ, 375, 121
Rastorguev, A.S., Pavlovskaya, E.D. Durlevich, O.V. & Filippova, A.A. 1994, AstL, 20, 591
Reid, M.J. 1993, ARA&A, 31, 345
Rice, W., Merrill, K.M., Gatley, I. & Gillett, F.C. 1996, AJ, 112, 114
Robin, A.C., Reylé, C. & Crézé, M. 2000, A&A, 359, 103
Rosenberg, A., Saviane, I., Piotto, G. & Aparicio, A. 1999. AJ, 118, 2306
Salaris, M. & Weiss, A. 2002, A&A, 388, 492
Sandage, A. 1990, JRASC, 84, 70
Schlegel, D.J., Finkbeiner, D.P. & Davis, M. 1998, ApJ, 500, 525
Searle, L. & Zinn, R. 1978, ApJ, 225, 357
Sérsic, J.L. 1966, in *Atlas de Galaxias Australes*; Observatorio Astronomico de Córdoba, p.141
Siegel, M.H., Majewski, S.R., Cudworth, K.M. & Takamiya, M. 2001, AJ, 121, 935
Sumi, T. 2004, MNRAS, 349, 193
Vesperini, E. & Heggie, D.C. 1997, MNRAS, 289, 898
Willman, B., Blanton, M.R., West, A.A. et al., 2005, AJ, 129, 2692
Yanny, B., Newberg, H.J., Kent, S. et al. 2000, ApJ, 540, 825
Zepf, S.E., Carter, D., Sharples, R.M. & Ashman, K. 1995, ApJL, 445, 19
Zinn, R. 1980, ApJ, 241, 602
Zinn, R. 1985, ApJ, 293, 424
Zinn, R. 1993, in *The Globular Cluster-Galaxy Connection*, eds. Smith, G.H. and Brodie, J.P., ASP Conf. Ser. 48, Astron. Soc. Pac., San Francisco, p.38

Table 1. Updated Globular Cluster parameters - the GC05 sample

GC	ℓ	b	E(B-V)	[Fe/H]	$d_\odot$	d_{GC}	d_{GC}	Heliocentric x	y	z	Notes	Alternative designations
	(°)	(°)			(kpc)	(kpc)	(kpc)	(kpc)	(kpc)	(kpc)		
(1)	(2)	(3)	(4)	(5)	(6)	(7)	(8)	(9)	(10)	(11)	(12)	(13)
NGC6723	0.07	-17.30	0.05	-1.12	8.8	2.6	2.9	8.40	0.01	-2.62		GCl-106,ESO396SC10
NGC6287	0.13	11.02	0.60	-2.05	8.5	1.7	2.0	8.34	0.02	1.62		GCl-54,ESO518SC10
NGC6558	0.20	-6.03	0.44	-1.44	7.4	1.0	0.8	7.36	0.03	-0.78		Mel-194,Cr368,OCl-3,GCl-89,ESO456SC62
NGC6569	0.48	-6.68	0.55	-0.86	8.7	1.2	1.7	8.64	0.07	-1.01		GCl-91,ESO456SC77
Pal5	0.85	45.86	0.03	-1.41	23.2	18.6	18.9	16.16	0.24	16.65	Y^{11}	Serpens,GCl-32
NGC6325	0.97	8.00	0.89	-1.17	9.6	2.0	2.6	9.51	0.16	1.34		GCl-58,ESO519SC11
NGC6522	1.02	-3.93	0.48	-1.44	7.8	0.6	0.8	7.78	0.14	-0.53		GCl-82,ESO456SC43
NGC6528	1.14	-4.17	0.54	-0.04	9.1	1.3	2.0	9.07	0.18	-0.66		GCl-84,ESO456SC48
NGC6652	1.53	-11.38	0.09	-0.96	9.6	2.4	2.9	9.41	0.25	-1.89		GCl-98,ESO395SC11
M69	1.72	-10.27	0.16	-0.70	8.6	1.6	2.0	8.46	0.25	-1.53		NGC6637,GCl-96,ESO457SC14
Pal6	2.09	1.78	1.46	-1.09	7.3	0.8	0.4	7.29	0.27	0.23		GCl-75,ESO520SC21
ESO456SC38	2.76	-2.51	0.89	-0.50	6.7	1.4	0.7	6.69	0.32	-0.29		Djorgovski2
NGC6624	2.79	-7.91	0.28	-0.44	8.0	1.2	1.4	7.91	0.39	-1.10		GCl-93,ESO457SC11
M70	2.85	-12.51	0.07	-1.51	9.0	2.1	2.5	8.78	0.44	-1.95		NGC6681,GCl-101,ESO458SC3
NGC6540	3.29	-3.31	0.60	-1.20	3.7	4.4	3.5	3.69	0.21	-0.21		Cr364,OCl-11,ESO456SC53,Djorgovski3
M107	3.37	23.01	0.33	-1.04	6.4	3.3	2.9	5.89	0.35	2.50		NGC6171,GCl-44
Tz7	3.39	-20.07	0.07	-0.58	23.2	16.0	16.6	21.75	1.29	-7.96	$S^{1,9}Y^{3,11}$	ESO397SC14
NGC6401	3.45	3.98	0.72	-0.98	7.7	0.8	0.8	7.67	0.46	0.53		GCl-73,ESO520SC11
Tz9	3.60	-1.99	1.87	-2.00	7.7	0.6	0.7	7.68	0.48	-0.27		ESO521SC11
Tz5	3.81	1.67	2.15	0.00	7.6	0.7	0.7	7.58	0.50	0.22		Tz11,ESO520SC26,ESO520SC27
M5	3.86	46.80	0.03	-1.27	7.5	6.2	5.9	5.12	0.35	5.47		NGC5904,GCl-34
Tz10	4.42	-1.86	2.40	-0.70	5.7	2.4	1.6	5.68	0.44	-0.19		ESO521SC16
NGC6342	4.90	9.73	0.46	-0.65	8.6	1.7	2.0	8.45	0.72	1.45		GCl-61,ESO587SC6
UKS1	5.12	0.76	3.09	-0.50	8.3	0.8	1.3	8.27	0.74	0.11		
NGC6553	5.25	-3.02	0.63	-0.21	5.6	2.5	1.7	5.67	0.51	-0.30		GCl-88,ESO521SC36
M9	5.54	10.70	0.38	-1.75	8.2	1.7	1.9	8.02	0.78	1.52		NGC6333,GCl-60,ESO587SC5
M54	5.61	-14.09	0.15	-1.58	19.6	27.2	12.8	18.92	1.86	-4.77	$S^{1,9}DN^2$	NGC6715,GCl-104,ESO458SC8
Tz8	5.76	-24.56	0.12	-2.00	26.0	19.1	19.7	23.53	2.37	-10.81	$S^{1,9}$	ESO398SC21
NGC6544	5.84	-2.20	0.73	-1.56	2.6	5.4	4.6	2.58	0.26	-0.10		Mel-192,Cr366,OCl-17,GCl-87,ESO521SC28
NGC6356	6.72	10.22	0.28	-0.50	15.2	7.6	8.3	14.86	1.75	2.70		GCl-62,ESO588SC1
NGC6440	7.73	3.80	1.07	-0.34	8.4	1.3	1.7	8.31	1.13	0.56		GCl-77,ESO589SC8
M28	7.80	-5.58	0.40	-1.45	5.7	2.6	1.9	5.62	0.77	-0.55		NGC6626,GCl-94,ESO522SC23
NGC6638	7.90	-7.15	0.40	-0.99	8.4	1.6	1.9	8.26	1.15	-1.05		GCl-95,ESO522SC30
Tz12	8.36	-2.10	2.06	-0.50	4.8	3.4	2.6	4.75	0.70	-0.18		ESO522SC1
Arp2	8.55	-20.78	0.10	-1.76	28.6	21.4	22.1	26.44	3.98	-10.15	$S^{1,9}Y^3$	GCl-112,ESO460SC6
M55	8.80	-23.27	0.08	-1.81	5.4	3.8	3.2	4.90	0.76	-2.13		NGC6809,GCl-113,ESO460SC21
2MASS-GC02	9.78	-0.62	5.56	—	4.0	—	3.4	3.94	0.68	-0.04		
NGC6642	9.81	-6.44	0.41	-1.35	7.7	1.6	1.6	7.54	1.30	-0.86		Mel-203,Cr381,OCl-29,GCl-97,ESO522SC32
M22	9.89	-7.55	0.34	-1.64	3.2	4.9	4.1	3.12	0.54	-0.42		NGC6656,GCl-99,ESO523SC4
2MASS-GC01	10.47	0.1	6.80	-1.20	3.6	—	3.7	3.54	0.65	0.01		
NGC6717	12.88	-10.9	0.22	-1.29	7.4	2.3	2.1	7.08	1.62	-1.40		Pal9,Cr395,OCl-37,GCl-105,ESO523SC14
Pal8	14.10	-6.80	0.32	-0.48	12.9	5.6	6.3	12.42	3.12	-1.53		GCl-100,ESO591SC12
M10	15.14	23.08	0.28	-1.52	4.4	4.6	3.9	3.91	1.06	1.72		NGC6254,GCl-49
M12	15.72	26.31	0.19	-1.48	4.9	4.5	3.9	4.23	1.19	2.17		NGC6218,GCl-45
IC1257	16.53	15.14	0.73	-1.70	25.0	17.9	18.5	16.13	6.87	6.53		OCl-51
NGC6366	18.41	16.04	0.71	-0.82	3.6	5.0	4.2	3.28	1.09	0.99	Y^{11}	GCl-65
Pal15	18.87	24.30	0.40	-1.90	44.6	37.9	38.5	38.46	13.15	18.35		GCl-50
NGC6517	19.23	6.76	1.08	-1.37	10.8	4.3	4.7	10.13	3.53	1.27		GCl-81
M75	20.30	-25.75	0.16	-1.16	18.8	12.8	13.3	15.88	5.87	-8.17	R^5	NGC6864,GCl-116,ESO595SC13
NGC6539	20.80	6.78	0.97	-0.66	8.4	3.1	3.2	7.80	2.96	0.99		GCl-85
M14	21.32	14.81	0.60	-1.39	8.9	3.9	3.9	8.02	3.13	2.27		NGC6402,GCl-72
IC1276	21.83	5.67	1.08	-0.73	5.4	3.7	3.0	4.99	2.00	0.53		Pal7,GCl-90
NGC6712	25.35	-4.32	0.45	-1.01	6.9	3.5	3.1	6.22	2.95	-0.52		Mel-215,OCl-72,GCl-103
M30	27.18	-46.83	0.03	-2.12	8.0	7.1	6.8	4.87	2.50	-5.83	R^5	NGC7099,GCl-122,ESO531SC21
NGC6535	27.18	10.44	0.34	-1.80	6.7	3.9	3.5	5.86	3.01	1.21		GCl-83
NGC6426	28.09	16.23	0.36	-2.26	20.4	14.2	14.8	17.28	9.22	5.70		Cr346,OCl-81,GCl-76
Pal14	28.75	42.18	0.04	-1.52	73.9	69.0	69.4	48.01	26.34	49.62		AvdB,Arp1,GCl-38
Pal12	30.51	-47.68	0.02	-0.94	19.1	15.9	16.0	11.08	6.53	-14.12	$Y^{3,11}ST^9$	Capricornus,GCl-123,ESO600SC11
GLIMPSE-C01	31.30	-0.10	4.84	—	3.1	6.8	4.8	2.65	1.61	-0.01		
Pal11	31.81	-15.58	0.35	-0.39	12.9	7.8	8.1	10.56	6.55	-3.46		GCl-114
M72	35.16	-32.68	0.05	-1.40	17.0	12.9	13.1	11.70	8.24	-9.18	R^5	NGC6981,GCl-118
NGC6760	36.11	-3.92	0.77	-0.52	7.4	4.8	4.6	5.96	4.35	-0.51		Mel-219,OCl-92,GCl-109
NGC6749	36.20	-2.20	1.50	-1.60	7.9	5.0	4.7	6.37	4.66	-0.30		Be42,OCl-91,GCl-107
NGC5466	42.15	73.59	0.00	-2.22	17.0	17.2	17.0	3.56	3.22	16.31		GCl-27
M3	42.21	78.71	0.01	-1.57	10.4	12.2	11.8	1.51	1.37	10.20		NGC5272,GCl-25
NGC6934	52.10	-18.89	0.10	-1.54	17.4	14.3	14.4	10.11	12.99	-5.63	$R^{5,12}Y^{11}$	GCl-117
Pal10	52.44	2.72	1.66	-0.10	5.9	6.4	5.9	3.59	4.67	0.28		GCl-111
M2	53.38	-35.78	0.06	-1.62	11.5	10.4	10.2	5.56	7.49	-6.72		NGC7089,GCl-121
NGC7492	53.39	-63.48	0.00	-1.51	25.8	24.9	24.9	6.87	9.25	-23.09	R^5	Mel-242,OCl-111,GCl-125
M71	56.74	-4.56	0.25	-0.73	3.9	6.7	6.0	2.13	3.25	-0.31		NGC6838,Mel-226,Cr409,OCl-117,GCl-115
M13	59.01	40.91	0.02	-1.54	7.7	8.7	8.2	3.00	4.99	5.04	R^5	NGC6205,GCl-44
M56	62.66	8.34	0.20	-1.94	10.1	9.7	9.4	4.59	8.88	1.46	R^{12}	NGC6779,GCl-110
NGC7006	63.77	-19.41	0.05	-1.63	41.5	38.8	39.0	17.30	35.11	-13.79	R^5	GCl-119
M15	65.01	-27.31	0.10	-1.62	10.3	10.4	10.1	3.87	8.30	-4.73		NGC7078,GCl-120
M92	68.34	34.86	0.02	-2.28	8.2	9.6	9.1	2.48	6.25	4.69		NGC6341,GCl-59
NGC6229	73.64	40.31	0.01	-1.43	30.7	30.0	30.0	6.59	22.46	19.86		GCl-47
Pal13	87.10	-42.70	0.05	-1.74	26.9	27.8	27.6	1.00	19.74	-18.24	R^7	Pegasus,GCl-124
Pal1	130.07	19.03	0.15	-0.60	10.9	17.0	16.3	-6.63	7.89	3.55	Y^3CT^9	GCl-6
NGC288	152.28	-89.38	0.03	-1.24	8.3	11.6	11.0	-0.08	0.04	-8.30	R^8	GCl-2,ESO474SC37
SDSSJ1049+5103†	155.65	55.62	0.01**	-1.70*	45.0	50.0	49.1	-23.15	10.48	37.14		
Whiting 1‡	161.62	-60.64	0.04	-1.20	45.0	—	48.1	-20.94	6.96	-39.22	Y^4	WHI,B0200-03
Pal2	170.53	-9.07	1.24	-1.30	27.6	35.4	34.7	-26.88	4.48	-4.35		GCl-7
NGC2419	180.37	25.24	0.11	-2.12	84.2	91.5	90.8	-76.16	-0.49	35.90	DN^2	GCl-12

Table 1. Continued

GC	ℓ	b	E(B-V)	[Fe/H]	$d_\odot$	d_{GC}	d_{GC}	Heliocentric x	y	z	Notes	Alternative designations
	(°)	(°)			(kpc)	(kpc)	(kpc)	(kpc)	(kpc)	(kpc)		
(1)	(2)	(3)	(4)	(5)	(6)	(7)	(8)	(9)	(10)	(11)	(12)	(13)
Pal4	202.31	71.80	0.01	-1.48	109.2	111.8	111.5	-31.55	-12.95	103.74	Y^{11}	Ursa Majoris,GCl-17
Eridanus	218.11	-41.33	0.02	-1.46	90.2	95.2	94.6	-53.29	-41.80	-59.57	Y^{11}	ESO551SC1,C0422-213
M79	227.23	-29.35	0.01	-1.57	12.9	18.8	18.1	-7.64	-8.25	-6.32	C^9	NGC1904,GCl-10,ESO487SC7
Pal3	240.14	41.86	0.04	-1.66	92.7	95.9	95.6	-34.37	-59.88	61.86	Y^{11}	SextansC
NGC1851	244.51	-35.04	0.02	-1.22	12.1	16.7	16.1	-4.26	-8.94	-6.95	$Y^{11}C^9R^5$	GCl-9,ESO305SC16
NGC2298	245.63	-16.01	0.14	-1.85	10.7	15.7	15.1	-4.24	-9.37	-2.95	C^9	GCl-11,ESO366SC22
NGC4147	252.85	77.19	0.02	-1.83	19.3	21.3	21.0	-1.26	-4.09	18.82	R^5ST^9	GCl-18
AM1	258.36	-48.47	0.00	-1.80	121.9	123.2	123.1	-16.31	-79.16	-91.26		E1,ESO201SC10
Pyxis	261.32	7.00	0.21	-1.30	39.4	41.4	41.1	-5.90	-38.66	4.80		Weinberger3
NGC1261	270.54	-52.13	0.01	-1.35	16.4	18.2	17.9	0.09	-10.07	-12.95	Y^{11}	GCl-5,ESO155SC11
NGC3201	277.23	8.64	0.23	-1.58	5.2	9.0	8.4	0.65	-5.10	0.78	$R^{5,6}$	GCl-15,ESO263SC26
NGC2808	282.19	-11.25	0.22	-1.15	9.3	11.0	10.5	1.93	-8.92	-1.81	C^9Y^{11}	GCl-13,ESO91SC1
E3	292.27	-19.02	0.30	-0.80	4.3	7.6	6.9	1.54	-3.76	-1.40		ESO37SC1
M68	299.63	36.05	0.05	-2.06	10.2	10.1	9.9	4.08	-7.17	6.00		NGC4590,GCl-20,ESO506SC30
Ru106	300.89	11.67	0.20	-1.67	21.2	18.5	18.6	10.66	-17.82	4.29	Y^3	OCl-887,ESO218SC10
NGC4372	300.99	-9.88	0.39	-2.09	5.8	7.1	6.6	2.94	-4.90	-1.00		GCl-19,ESO64SC6
NGC362	301.53	-46.25	0.05	-1.16	8.5	9.3	8.9	3.07	-5.01	-6.14	$Y^{11}R^{12}$	GCl-3,ESO51SC13
NGC4833	303.61	-8.01	0.32	-1.80	6.0	6.9	6.4	3.29	-4.95	-0.84		GCl-21,ESO65SC4
47 Tucanae	305.90	-44.89	0.04	-0.76	4.5	7.4	6.7	1.87	-2.58	-3.18		NGC104,GCl-1,ESO50SC9
IC4499	307.35	-20.47	0.23	-1.60	18.9	15.7	15.9	10.74	-14.08	-6.61	Y^3	GCl-30,ESO22SC5
ω Centauri	309.10	14.97	0.12	-1.62	5.3	6.4	5.8	3.23	-3.97	1.37	DN^2R^{12}	NGC5139,GCl-24,ESO270SC11
NGC5286	311.61	10.57	0.24	-1.67	11.0	8.4	8.3	7.18	-8.08	2.02	CT^9	GCl-26,ESO220SC38
NGC6101	317.75	-15.82	0.05	-1.82	15.3	11.1	11.3	10.90	-9.90	-4.17		GCl-40,ESO69SC4
AM4	320.28	33.51	0.04	-2.00	29.9	25.5	25.9	19.18	-15.93	16.51		AM1353-265
NGC6362	325.55	-17.57	0.09	-0.95	8.1	5.3	5.1	6.37	-4.37	-2.45		GCl-66,ESO102SC8
NGC5927	326.60	4.86	0.45	-0.37	7.6	4.5	4.3	6.32	-4.17	0.64		GCl-35,ESO224SC4
NGC5946	327.58	4.19	0.54	-1.38	12.8	7.4	7.8	10.78	-6.84	0.94		IC4550,GCl-36,ESO224SC7
BH176	328.41	4.34	0.77	-0.13	14.5	8.8	9.2	12.32	-7.57	1.10	Y^{10}	ESO224SC8
Lynga7	328.77	-2.79	0.73	-0.62	7.2	4.2	3.9	6.15	-3.73	-0.35		OCl-949,BH184,ESO178SC11
NGC5694	331.06	30.36	0.09	-1.86	34.7	29.1	29.6	26.20	-14.49	17.54		GCl-29,ESO512SC10
NGC5824	332.55	22.07	0.13	-1.85	32.0	25.8	26.4	26.32	-13.67	12.02		GCl-31,ESO387SC1
M53	332.96	79.76	0.02	-1.99	18.3	18.8	18.6	2.90	-1.48	18.01		NGC5024,GCl-22
NGC5053	335.69	78.94	0.04	-2.29	16.4	16.9	16.7	2.87	-1.30	16.10		Cr267,OCl-970,GCl-23
NGC6752	336.50	-25.63	0.04	-1.56	4.0	5.2	4.5	3.31	-1.44	-1.73		GCl-108,ESO141SC30
NGC5986	337.02	13.27	0.28	-1.58	10.5	4.8	5.1	9.41	-3.99	2.41		GCl-37,ESO329SC18
NGC6397	338.17	-11.96	0.18	-1.95	2.3	6.0	5.2	2.09	-0.84	-0.48		GCl-74,ESO181SC4
NGC6352	341.42	-7.17	0.21	-0.70	5.7	3.3	2.7	5.36	-1.80	-0.71	Y^{11}	Mel-170,Cr328,OCl-993,GCl-64,ESO228SC3
NGC6584	342.14	-16.41	0.10	-1.49	13.4	7.0	7.4	12.23	-3.94	-3.79		GCl-92,ESO229SC14
NGC5634	342.21	49.26	0.05	-1.88	25.9	21.9	22.1	16.09	-5.16	19.62		GCl-28
NGC6139	342.37	6.94	0.75	-1.68	10.1	3.6	4.0	9.56	-3.04	1.22		GCl-43,ESO331SC4
NGC5897	342.95	30.29	0.09	-1.80	12.8	7.7	8.0	10.57	-3.24	6.46		GCl-33,ESO582SC2
Tz3	345.08	9.19	0.72	-0.73	7.5	2.4	2.2	7.15	-1.91	1.20		ESO390SC6
NGC6388	345.56	-6.74	0.37	-0.60	11.5	4.4	5.0	11.06	-2.85	-1.35		GCl-70,ESO279SC2
ESO280SC6	346.90	-12.57	0.07	-2.00	21.7	14.5	15.0	20.63	-4.80	-4.72		
NGC6256	347.79	3.31	1.03	-0.70	6.6	2.1	1.6	6.44	-1.39	0.38		BH208,ESO391SC6
NGC6496	348.02	-10.01	0.15	-0.64	11.5	4.3	4.9	11.08	-2.35	-2.00		GCl-80,ESO279SC13
NGC6541	349.29	-11.18	0.14	-1.83	7.0	2.2	1.9	6.75	-1.28	-1.36		GCl-86,ESO280SC4
NGC6380	350.18	-3.42	1.17	-0.50	10.7	3.2	3.8	10.52	-1.82	-0.64		Ton1,Pis25,GCl-68,BH233,ESO333SC14
Ton2	350.80	-3.42	1.24	-0.50	8.1	1.4	1.6	7.98	-1.29	-0.48		Pis26,GCl-71,BH236,ESO333SC16
M4	350.97	15.97	0.36	-1.20	2.2	5.9	5.2	2.09	-0.33	0.61		NGC6121,GCl-41,ESO517SC1
ESO452SC11	351.91	12.1	0.49	-1.50	7.8	2.0	2.0	7.55	-1.07	1.64		C1636-283
NGC6144	351.93	15.70	0.36	-1.75	10.3	3.6	4.1	9.82	-1.39	2.79		GCl-42,ESO517SC6
M80	352.67	19.46	0.18	-1.75	10.0	3.8	4.1	9.35	-1.20	3.33		NGC6093,GCl-39,ESO516SC11
NGC6441	353.53	-5.01	0.47	-0.53	11.2	3.5	4.2	11.09	-1.26	-0.98		GCl-78,ESO393SC34
M62	353.58	7.32	0.47	-1.29	6.9	1.7	1.2	6.80	-0.77	0.88		NGC6266,GCl-51,ESO453SC14
Liller1	354.84	-0.16	3.06	0.22	10.5	2.6	3.4	10.46	-0.94	-0.03		
NGC6453	355.72	-3.87	0.66	-1.53	11.2	3.3	4.1	11.14	-0.83	-0.76		GCl-79,ESO393SC36
NGC6304	355.83	5.38	0.53	-0.59	6.1	2.1	1.4	6.06	-0.44	0.57		GCl-56,ESO454SC2
Tz4	356.02	1.31	2.35	-1.60	9.1	1.3	2.0	9.08	-0.63	0.21		HP4,ESO454SC7
Tz2	356.32	2.30	1.57	-0.40	8.7	0.9	1.6	8.68	-0.56	0.35		HP3,BH228,ESO454SC29
Djorgovski1	356.67	-2.48	1.44	-2.00	8.8	1.0	1.7	8.78	-0.51	-0.38		
M19	356.87	9.38	0.41	-1.68	8.7	1.6	2.0	8.57	-0.47	1.42		NGC6273,GCl-52,ESO518SC7
NGC6316	357.18	5.76	0.51	-0.55	11.0	3.2	3.9	10.93	-0.54	1.10		GCl-57,ESO454SC4
HP1	357.42	2.12	0.74	-1.55	7.4	0.8	0.5	7.39	-0.33	0.27		GCl-67,BH229,ESO455SC11
Tz1	357.57	1.00	2.28	-1.30	6.2	1.8	1.1	6.19	-0.26	0.11		HP2,GCl-69,ESO455SC23
NGC6293	357.62	7.83	0.41	-1.92	8.8	1.4	1.9	8.71	-0.36	1.20		GCl-55,ESO519SC5
NGC6284	358.35	9.94	0.28	-1.32	14.7	6.9	7.7	14.47	-0.42	2.54		GCl-53,ESO518SC9
Tz6	358.57	-2.16	2.14	-0.50	9.5	1.6	2.3	9.49	-0.24	-0.36		HP5,BH249,ESO393SC36,BDSB103
NGC6235	358.92	13.52	0.36	-1.40	10.0	2.9	3.4	9.72	-0.18	2.34		GCl-58,ESO519SC11
NGC6355	359.58	5.43	0.75	-1.50	7.2	1.0	0.7	7.17	-0.05	0.68		Cr330,OCl-1036,GCl-63,ESO519SC15

Table Notes. S: Sagittarius; C: Canis Major; Y: Younger than 10 Gyr; R: Retrograde orbit; DN: Dwarf nucleus; ST: Sagittarius tidal tail; CT: Canis Major tidal tail. (1) - da Costa & Armandroff (1995); (2) - Mackey & van den Bergh (2005); (3) - Rosenberg et al. (1999); (4) - Carraro (2005); (5) - van den Bergh (1993); (6) - Coté et al. (1995); (7) - Siegel et al. (2001); (8) - Guo et al. (1993); (9) - Forbes, Strader & Brodie (2004); (10) - Phelps & Schick (2003); (11) - Salaris & Weiss (2002); (12) - Dinescu, Girard & van Altena (1999). (†) and (‡) cluster parameters from Willman, Blanton & West et al. (2005) and Carraro (2005), respectively. (∗): based on the conclusion by Willman, Blanton & West et al. (2005) that the cluster is more metal-poor than Pal 5; (∗∗): based on Schlegel, Finkbeiner & Davis (1998). Col. 7: Galactocentric distance from H03. Col.8 : this work.